Technology in Cancer Research & Treatment
Volume 23: 1-14
© The Author(s) 2024
Article reuse guidelines:
sagepub.com/journals-permissions
DOI: 10.1177/15330338241285158
journals.sagepub.com/home/tct

First-In-DOg HISTotripsy for Intracranial Tumors Trial: The FIDOHIST Study

Christina Vezza, DVM[1,*], Lauren Ruger, PhD[2,*], Maya Langman, MD[3], Elliana Vickers[4], Francesco Prada, MD[5,6], Jonathan Sukovich, PhD[7], Timothy Hall, PhD[7], Zhen Xu, PhD[7], Rell L. Parker, DVM, PhD[1], Eli Vlaisavljevich, PhD[2], and John H. Rossmeisl, DVM[1]

Abstract

Objective: Brain tumors represent some of the most treatment refractory cancers, and there is a clinical need for additional treatments for these tumors. Domesticated dogs are the only other mammalian species which commonly develop spontaneous brain tumors, making them an ideal model for investigating novel therapies. Histotripsy is a non-thermal ultrasonic ablation method that emulsifies tissue through acoustic cavitation. The primary objectives of this prospective study were to assess the feasibility and safety of histotripsy to ablate naturally occurring canine brain tumors. Secondary endpoints included characterization of magnetic resonance imaging (MRI) responses to histotripsy treatment, and exploratory immunogenomic tumor response analyses. **Methods:** The study design utilized a treat and resect paradigm, where tumors were approached using craniotomy, partially ablated with histotripsy delivered through the cranial defect, imaged with MRI, and then resected. Dogs were evaluated with clinical, brain MRI, immunopathologic, and genomic examinations before treatment, intraoperatively, and 1, 14, and 42 days post-treatment. Here we report the results of the three dogs with meningiomas, all of which were treated with a custom eight element 1 MHz histotripsy transducer at a pulse repetition frequency of 100 Hz and a treatment dosage of 400 pulses/point. **Results:** Histotripsy was successfully delivered to all dogs, resulting in histopathologic evidence of ablations that were sharply demarcated from untreated tumor, with measured treatments approximating planned volumes in 2/3 dogs. One dog experienced an adverse event consisting of transient cerebral edema that was possibly attributable to histotripsy. Histotripsy ablations could be grossly visualized and identified on MRI, with features consistent with hemorrhage and necrosis. Significant expression or upregulation of the damage associated molecular pattern HMGB1, cytokine-cytokine receptor interaction, and NF-κb signaling pathways were observed in histotripsy treated tumors. **Conclusion:** Ablation of canine meningiomas with histotripsy through an open cranial window was feasible and clinically well tolerated.

Keywords

canine, brain tumor, focused ultrasound, histotripsy, meningioma, tumor ablation

[1] Department of Small Animal Clinical Sciences, Virginia-Maryland College of Veterinary Medicine, Virginia Polytechnic Institute and State University, Blacksburg, VA, USA
[2] Department of Biomedical Engineering and Mechanics, Virginia Polytechnic Institute and State University, Blacksburg, VA, USA
[3] Department of Neurosurgery, Medical College of Wisconsin, Milwuakee, WI, USA
[4] Graduate Program in Translational Biology, Medicine, and Health, Virginia Polytechnic Institute and State University, Roanoke, VA, USA
[5] Department of Neurosurgery, Fondazione IRCCS Istituto Neurologico C. Besta, Milano, Italy
[6] Departement of Neurological Surgery, University of Virginia, Charlottesville, VA, USA
[7] Department of Biomedical Engineering, University of Michigan, Ann Arbor, MI, USA

*Authors contributed equally to this work.

Corresponding Author:
John H. Rossmeisl, Department of Small Animal Clinical Sciences, 205 Duckpond Drive, Virginia-Maryland College of Veterinary Medicine, Virginia Polytechnic Institute and State University, Blacksburg, VA, USA 24061.
Email: jrossmei@vt.edu



Creative Commons Non Commercial CC BY-NC: This article is distributed under the terms of the Creative Commons Attribution-NonCommercial 4.0 License (https://creativecommons.org/licenses/by-nc/4.0/) which permits non-commercial use, reproduction and distribution of the work without further permission provided the original work is attributed as specified on the SAGE and Open Access page (https://us.sagepub.com/en-us/nam/open-access-at-sage).

Introduction

Over 1.3 million people in the United States are currently living with a brain tumor, and approximately 17,000 Americans die as a result of brain tumors each year.[1] Surgical resection remains a primary therapeutic approach used for benign and malignant brain tumors, both as a singular modality and in combination with other treatments. However, not all tumors are amenable to surgery, and subtotal tumor resection leading to tumor recurrence continues to be problematic, being associated with patient morbidity and death.[2,3] In addition, the median survival of patients with the most common malignant brain tumor, glioblastoma, is only 18 months following multimodality therapy, highlighting the need for improved treatments.[3]

Dogs are the only other mammalian species besides humans known to commonly develop brain tumors spontaneously, and canine tumors share many clinical, neuropathological, and cytogenetic features with human tumors.[4,5] This makes dogs an attractive model for pre-clinical testing of novel approaches to brain tumors, such as histotripsy. Histotripsy is a non-thermal ultrasonic ablation method being developed as an intervention for several types of cancers, including brain, liver, pancreatic, prostate, and sarcomas.[6–10] Histotripsy ablates tissue through the precise control of acoustic cavitation.[6] Using microsecond-long, high-pressure pulses, histotripsy generates a bubble cloud inside of a target tissue; these bubbles then rapidly expand and collapse to impart high mechanical strains on surrounding cells, emulsifying the treated region.[6] While it has been demonstrated that transcranial histotripsy can target locations throughout the brain, including locations near the skull surface, transcranial applications require costly and specialized neuronavigational guidance systems and advanced histotripsy devices able to overcome attenuation of the therapeutic ultrasound signal by the skull.[10,11]

To complement ongoing studies developing transcranial histotripsy systems and to expand available comparative data regarding the clinicopathological effects of histotripsy in the naturally diseased brain, here we investigate the feasibility and safety of treating spontaneous canine brain tumors with histotripsy through an open craniectomy under ultrasound guidance using a custom 8 element, 1 MHz histotripsy transducer mounted onto a prototype clinical histotripsy system.[9] We hypothesized that: 1) histotripsy could precisely ablate brain tumors, as defined histologically by evidence of necrosis within treated tumor volumes, without inducing collateral damage to adjacent brain structures; 2) histotripsy tumor ablations could be visualized and quantified using in vivo post-treatment magnetic resonance imaging (MRI) examinations; and 3) histotripsy treatment would result in the release of the damage associated molecular pattern high mobility group box 1 (HMGB1) from tumors.

Materials and Methods

Clinical Trial Protocol and Endpoints

The reporting of this study conforms to ARRIVE 2.0 guidelines.[12] Client-owned dogs with naturally occurring brain tumors were prospectively recruited from May 2022 - September 2023. All study procedures complied with the Guide for the Care and Use of Laboratory Animals and were approved by the Institutional Animal Care and Use Committee (protocol #20-190; approved November 20, 2020) and owners provided written informed consent for their dogs to participate. Individual animal care was provided according to best clinical practices for dogs with brain tumors in the context of an established veterinarian-client-patient relationship. For inclusion, dogs had to have clinical signs of brain disease, a baseline Karnofsky Performance Score (KPS) $\geq$ 70,[13,14] a diagnostic brain MRI scan demonstrating a solitary intracranial lesion with imaging characteristics compatible with a primary brain tumor that was amenable to surgical resection,[15] and no significant concurrent cardiopulmonary, renal, or hepatic disease or other malignancies. Dogs having received any type of prior brain radiotherapy or treatment with a cytotoxic chemotherapy drug within 6 weeks of trial enrollment were excluded.

The primary endpoints were to evaluate the technical feasibility and safety of histotripsy for the treatment of brain tumors. Feasibility was defined by success of technical delivery of histotripsy to the tumor via demonstration of histopathologic evidence of tumor ablation (necrosis) in the post-treatment samples.[14] Safety was defined as the absence of severe toxicity attributable to the histotripsy treatment within 14 days of the procedure. Severe toxicity was clinically defined by a $\geq$ 20 point decline in the KPS from pre-treatment values, or development of grades 3, 4, or 5 adverse events (AE), as classified and graded according to Veterinary Cooperative Oncology Group Common Terminology Criteria for Adverse Events.[16]

Secondary endpoints included characterization of the imaging features of histotripsy ablations and evidence of collateral damage to adjacent brain structures on post-treatment MRI examinations. Exploratory immunological analyses included immunohistochemical quantification of immune cells within tumors, quantification of peripheral blood and intratumoral concentrations of high mobility group box 1 (HMGB1) protein, and immunological gene expression profiling of tumors performed on pre- and post-treatment samples.

Clinical trial procedures and workflow are summarized in Figure 1. On the day of enrollment (day −1), baseline evaluations for each dog included physical and neurological examinations, pre-treatment KPS scoring, and laboratory examinations (complete blood count, serum biochemical profile, urinalysis, banked plasma for immunological analyses). On the day of histotripsy treatment (day 0), dogs were placed under general anesthesia (Supplemental Methods),[17] each dog underwent a surgical approach and craniectomy sufficient to expose the tumor for histotripsy and resection, and an incisional biopsy of the tumor was obtained. The histotripsy treatment was then applied (specific methods below) and post-treatment brain MRI obtained. Following completion of the

post-treatment MRI, the tumor was surgically resected, the surgical wound closed using standard techniques, and the dog recovered from anesthesia. After craniectomy, dogs were

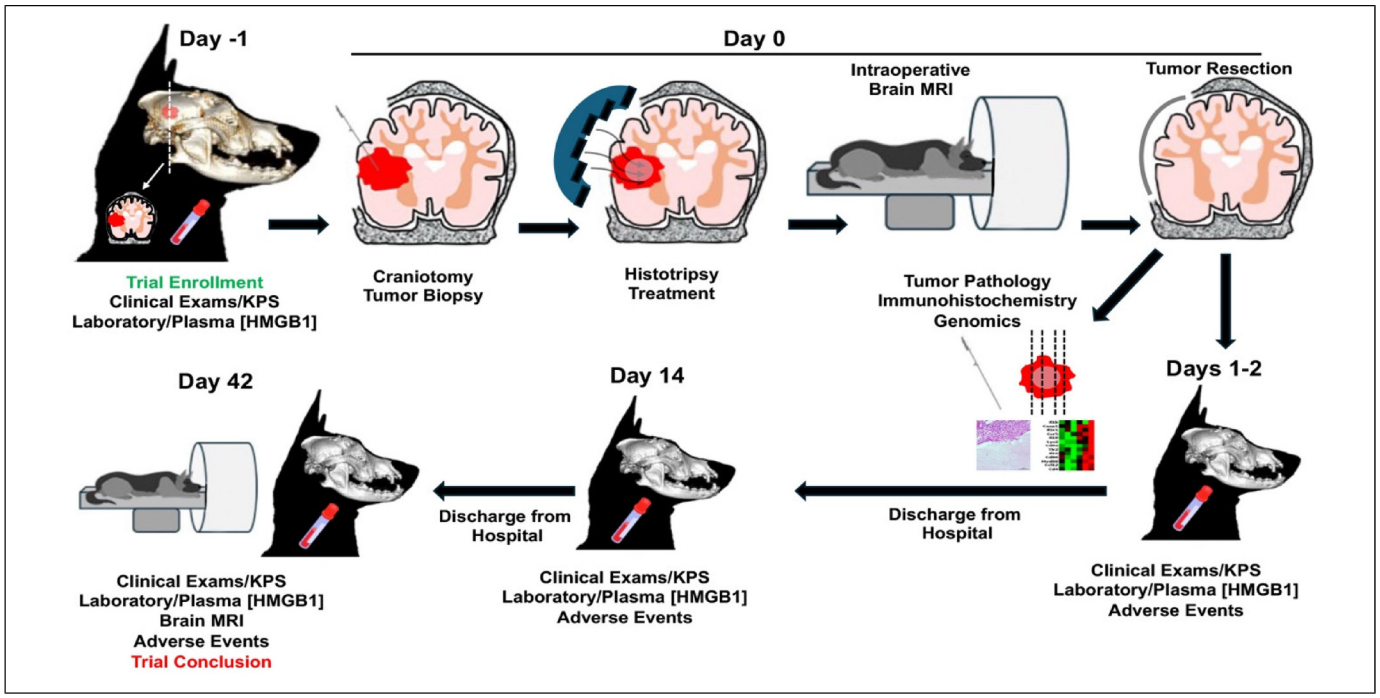


Figure 1. FIDOHIST study procedures and workflow.

recovered and monitored in the intensive care unit and received parenteral opioid analgesics for 24–48 h (Supplemental Methods).[17] On each day of hospitalization until discharge (days 1 and 2), dogs underwent physical and neurological examinations, post-treatment KPS scoring, laboratory monitoring, and AE monitoring. Dogs also received clinical, laboratory, and AE monitoring follow-up at 14 days post-treatment, and clinical, laboratory, AE monitoring, and a brain MRI examination under anesthesia on day 42 after treatment. Intraoperative (day 0) and post-treatment MRI (day 42; trial conclusion) were performed using a 1.5 T scanner (Intera, Philips Healthcare, Andover, MA, USA) and an 8-channel head coil with standardized sequences obtained as recommended for canine brain tumor trials (Supplemental Table S1).[18] Following completion of the trial, tumor surveillance or adjuvant therapeutic recommendations were made as appropriate by the attending clinician depending on each dog's tumor status.

Histotripsy System and Treatment

A custom 8-element, 1 MHz histotripsy transducer with a geometric focus of 45.5 mm and aperture size of 72.5 mm (f-number 0.63) was used for all histotripsy treatments (Figure 2**A**). A custom 4.9 MHz phased array ultrasound probe (PA 7-4, Analogic Corporation, Peabody, MA, USA) was coaxially aligned within the transducer for treatment guidance and monitoring; then, the transducer assembly was integrated onto a prototype clinical histotripsy system containing a computer-guided 3D robotic micropositioner (Histosonics, Ann Arbor, MI, USA) (Figure 2B). The transducer was driven via a high-voltage voltage amplifier designed to generate single cycle therapy pulses, controlled by an external function generator using 3 μs pulse waveforms (4063B Arbitrary Waveform Generator, B&K Precision, Yorba Linda, CA, USA), and powered by high and low voltage DC power supplies (GENH750 W, TDK-Lambda, National City, CA, USA).

To characterize the transducer output, focal pressure waveforms for the histotripsy transducer were measured in degassed water (Figure 2C) using a high-sensitivity reference rod hydrophone (HNR-0500, Onda Corp., Sunnyvale, CA, USA) and a cross-calibrated custom-built fiber optic probe hydrophone (FOPH) aligned at the transducer's focus as previously described prior to treatment.[19] Briefly, the rod hydrophone was used to measure the lateral, elevational, and axial 1-D beam profiles of the transducer at a peak negative pressure (p-) of ~2.2 MPa. The measured full-width half-maximum (FWHM) dimensions for the 1 MHz transducer were 1.4 mm, 1.35 mm, and 5.0 mm in the transverse, elevational, and axial directions, respectively. Then, focal pressures were measured directly with the FOPH up to a peak negative pressure of ~20 MPa. At peak negative pressures greater than 20 MPa, the focal pressure was linearly extrapolated using the collected data to prevent cavitation formation at the fiber tip. All waveforms were measured using a Tektronix TBS2000 series oscilloscope at a sample rate of 500MS/s, averaged over 512 pulses, and recorded in MATLAB (The MathWorks, Natick, MA, USA).

Prior to treatment, patient-specific treatment plans were designed based on ultrasound and MRI assessments. To visualize the tumor with ultrasound and guide the placement of the histotripsy transducer, once the craniectomy was completed in each dog, freehand imaging was completed using a linear ultrasound imaging probe with a frequency range of 10–18 MHz

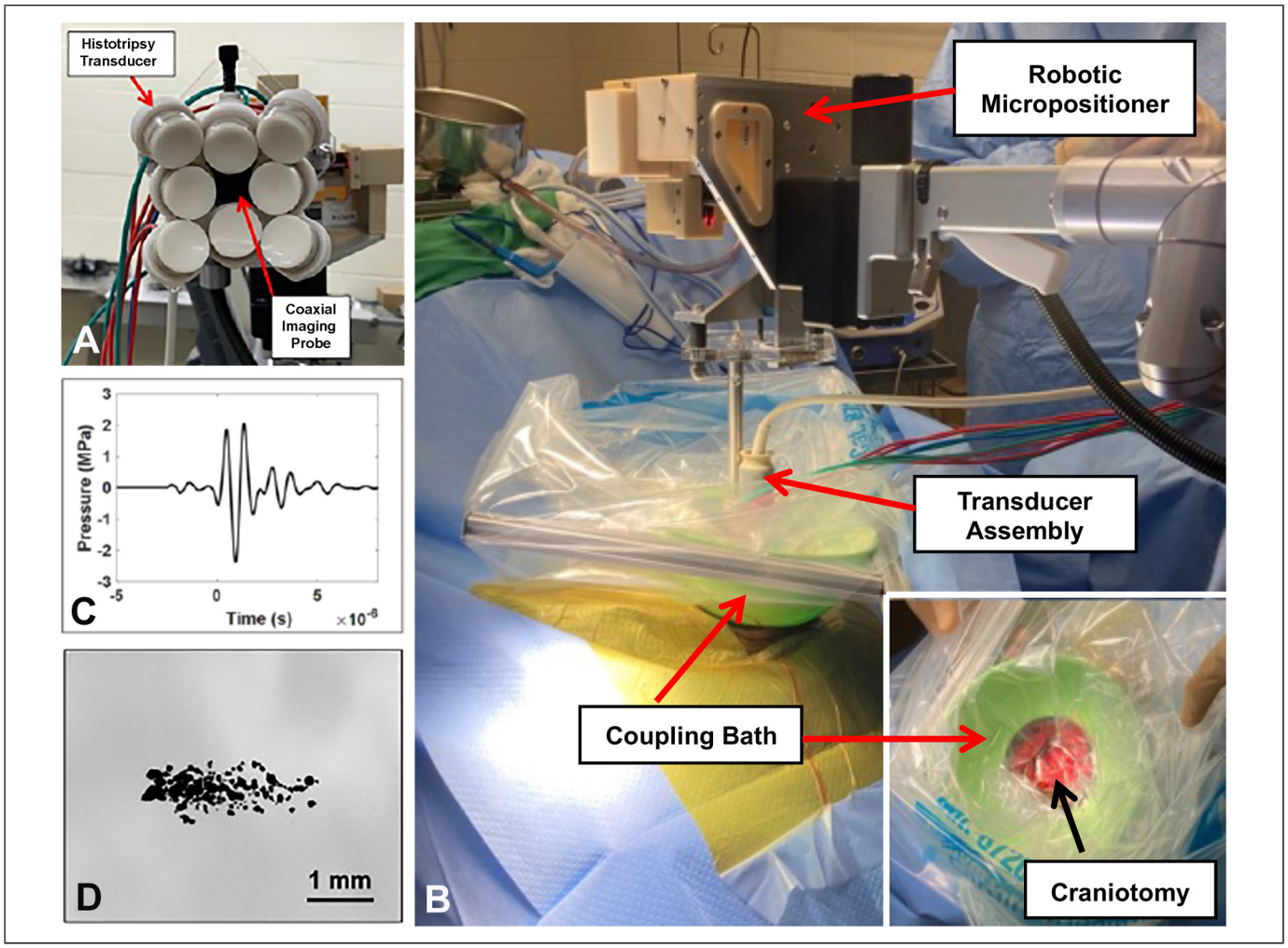


Figure 2. Histotripsy treatment approach and transducer characterization. A 1 MHz histotripsy transducer with a coaxially aligned imaging probe (A) was mounted onto a prototype clinical histotripsy system. (B) The histotripsy system consisted of a robotic positioner supporting the therapy and imaging transducer assembly and a water coupling bath (B). Representative pressure waveform (C) from the 1 MHz transducer collected at ~−2.4 MPa peak negative pressure using the rod hydrophone. Bubble cloud dimensions were measured to determine volumetric treatment spacing, with a representative bubble cloud at ~-40.5 MPa peak negative pressure shown (D).

(L18-10L30H-4, Telemed, Lithuania, Europe) wrapped in a sterile sleeve filled with coupling gel. Then, the histotripsy transducer was positioned over the craniectomy site and placed in a vessel of degassed water (<30% dissolved O_2) coupled to the canine patient to ensure acoustic propagation from the transducer to the brain (Figure 2B). Fine adjustments to correctly position the transducer over the targeted tumor region were made using the robotic positioner. It was originally intended to implant an acoustically transparent cranioplasty device (ATCI; Intelligenza Trasparente, Milan, Italy; Supplemental Figure S1) over each craniectomy defect and perform intraoperative ultrasound imaging and therapy and post-treatment ultrasonographic imaging of the treatment site through the implant.[19–21] However, the implant was found to substantially attenuate the acoustic energy able to be delivered with the histotripsy transducers being used, such that we were unable to deliver ablative pulses through the implant.[19] Thus, use of the implant for treatment was abandoned and all dogs subsequently received histotripsy directly through the open craniectomy defect. The ATCI was used for reconstructive cranioplasty purposes only in dog 2, but was not implanted in dogs 1 and 3.

Tumors were treated with histotripsy using single cycle pulses applied at a pulse repetition frequency (PRF) of 100 Hz. To determine the appropriate pressure level for treatment, the pressure at the focus was incrementally increased until a visible bubble cloud (Figure 2D) was generated on ultrasound imaging. Then, a spherical treatment volume completely contained within each tumor was manually defined using the clinical histotripsy system software before applying an automated volumetric treatment to a 3D grid of equidistant treatment points in the defined boundaries. The robotic positioner moved the focus between treatment locations, and each point was treated two times at a

treatment dosage of 200 pulses, resulting in a total dosage of approximately 400 pulses/point. All treatments were monitored in real time using ultrasound imaging and passive cavitation detection (PCD). For PCD monitoring, one of the transducer's therapy elements was connected to an oscilloscope with a high voltage probe. To detect the presence of cavitation in the focal region, the signal generated by the backscattering of the incident pulse from the focus was monitored as described previously.[9]

MRI Treatment Assessments

Qualitative and quantitative imaging characteristics of histotripsy treatment were performed by comparing pre-treatment to immediate post-treatment (day 0) MRI. MRI DICOM datasets from each dog and time were imported into image viewing and analysis software (Osirix MD, v11.0.4, Pixmeo, Switzerland). The contrast enhancing volume (CEV) of each dog's tumor (CEV) was calculated from each MRI obtained from all dogs using transverse 3DT1 W post-contrast images.[22] Manually defined regions of interest (ROIs) representing the CEV were generated on contiguous 3DT1 W image slices, and the subsequent CEV calculated with the Osirix MD ROI-volume function. Characterization of histotripsy induced lesions was performed by synchronizing and qualitatively comparing pre- to post-treatment image sequences. MRI derived histotripsy lesion volumes (mHLV) were determined from post-treatment transverse T2*GRE, using manually defined regions of interest (ROIs) generated on contiguous T2*GRE image slices, and the subsequent mHLV calculated with the Osirix MD ROI-volume function.

Tumor Pathology and Morphometry

Pre-treatment biopsies were divided into two sections, with one immersion fixed in 10% neutral buffered formalin and the other preserved in RNA Later (ThermoFisher, Waltham, MA, USA). Post-treatment resected tumors were mounted in a matrix slicer (Zivic Instruments, Pittsburg, PA, USA), serially sectioned and photographed in the transverse plane at 2 mm intervals, and macroscopically examined to identify regions of ablation.[14] Sections were obtained through ablated regions to evaluate the interface between treated and untreated tissues. At least one post-treatment section with gross evidence of ablation from each case was preserved in RNA Later, with the remaining tumor sections fixed in formalin. Formalin fixed tumor samples were processed routinely and stained with hematoxylin and eosin (H&E; Sakura Finetek, Torrance, CA, USA). Sections stained with H&E were used to grade tumors according to World Health Organization criteria modified for use in dogs, and to perform quantitative morphometric analysis.[14,23] Histologic ablation volumes (HAV) were obtained from serial sections using commercial image analysis software with a Cavalieri estimator (Stereo Investigator, MBF Biosciences, Williston, VT, USA).[14]

Exploratory Immunologic Assessments

- ***Plasma HMGB1 Enzyme Linked Immunoassay (ELISA)***

Concentrations of HMGB1 circulating in plasma were determined using a canine ELISA kit (LSF6302, LS Bio, Shirley, MA, USA) from samples obtained on study days −1, 1, 14, and 42, according to the manufacturer's instructions. Plasma HMGB1 assays were performed in this study, as increased circulating concentrations of HMGB1 have been previously observed following histotripsy treatment of other tumors, and recognition of this DAMP by pattern recognition receptors may be an initiator or facilitator of anti-tumor immune responses.[24] All samples were assayed in triplicate using 25 µl plasma samples, and optical densities were determined at 450 nm using a Spectramax 384 plate reader (Molecular Devices, San Jose, CA, USA). The manufacturer's stated detection range for HMGB1 is 6.25–400 pg/ml. To determine if plasma HMGB1 was elevated in tumor bearing dogs, or in dogs treated with histotripsy and surgery compared to conventional neurosurgical resection alone, concentrations of plasma HMGB1were quantified in six healthy, 2–3 year old Beagle dogs (3 male, 3 female) that received no therapeutic interventions and in samples obtained from an additional 3 dogs with meningiomas treated via conventional craniotomy and tumor resection. Longitudinal mixed models were used to compare plasma HMGB1 before and after treatment, with pre-treatment values included as covariates and time and treatment by time interactions examined. Statistical analyses were performed using SAS software. (v 9.0, Cary NC, USA).

- ***Western Blot- Intratumoral HMGB1***

Pre- (untreated) and post-treatment tumor extracts from all 3 dogs were prepared with SDS lysis buffer (Millipore Sigma, Burlington, MA, USA) and centrifuged at 14,000 × g for 10 min at 4 °C. The total protein concentration was determined using a bicinchoninic assay kit (BCA-1; Sigma-Aldrich, St Louis, MO, USA), and 40 µg of sample protein was separated under nonreducing conditions by 15% SDS-PAGE and transferred to PVDF membranes (Millipore Sigma). Two technical replicates were performed for each pre- and post-treatment tumor sample from each dog, and western blots were performed serially on each dog's pre- and post-tumor samples. After the membranes were blocked with 5% bovine serum albumin (ThermoFisher) for 1 h at room temperature, the blots were probed with rabbit polyclonal anti-human HMGB1 antibody, which cross reacts with canine HMGB1 (1:1500, LS-C140975, LS Bio). The membrane was rinsed and incubated with rabbit anti-IgG horseradish peroxidase conjugated secondary antibody (1:1000; R&D Systems, Minneapolis, MN, USA). A mouse monoclonal antibody to β-actin (1:1500, Abcam) was used as a protein loading control. Quantitative analyses were performed using a high-resolution

densitometric digital imaging (Amersham 600; GE Healthcare, Marlborough, MA, USA) and open source analytical software (Image J; United States National Institutes of Health, Bethesda, MD, USA). Associations between treatment status (pre- and post-treatment) and HMGB1 expression were assessed with the Wilcoxon rank sum test.

- ***Tumor Immunohistochemistry***

Immunohistochemistry for CD3 (A0452, Dako [Santa Clara, CA, USA], rabbit anti-human polyclonal, 1:150), CD4 (NBP1-19371, Novus Biologicals [Centennial, CO, USA], rabbit anti-human polyclonal, 1:100), CD8 (ab4055, Abcam [Waltham, MA, USA] rabbit anti-human polyclonal, 1:100), CD79a (HM57 Dako, mouse anti-human monoclonal, 1:50), FoxP3 (FJK-16 s; eBioscience [San Diego, CA, USA], rat anti-mouse, 1:50), Iba-1 (019-19741, Fujifilm Cellular Dynamics [Madison, WI, USA], rabbit anti-human polyclonal, 1:100), iNOS (ab15323, Abcam, rabbit polyclonal, 1:200), MHCII (F0817, Dako, mouse anti-human monoclonal, 1:2000) was performed on pre- and post-treatment tumor samples to evaluate the local immune response to histotripsy treatment. Immunohistochemical staining was run on a Ventana Benchmark XP (Roche, Indianapolis, IN, USA) automated system using universal discovery secondary antibodies (Roche), and an alkaline phosphatase red chromogenic detection kit with hematoxylin counterstain. All antibodies utilized have been previously validated for use in canine tissues.[25,26] Cell numbers for CD3, CD4, CD8, CD79a, FoxP3, Iba-1, and MHCII were quantified by counting immunolabeled cells in each of 10 high-power (400X) fields (hpf).[26] In the post-treatment samples, the fields selected for analysis included the tumor-treatment interface and areas entirely within the ablated region ($n = 5$ each). As cell counts did not display a normal distribution, Mann-Whitney tests were used to evaluate differences in cell populations between pre- and post-treatment tumor samples.

- ***Tumor Gene Expression***

mRNA expression profiling was performed on pre- and post-treatment formalin fixed paraffin-embedded (FFPE) tumor samples from all dogs. FFPE tissues were utilized for RNA profiling as inadequate sample volumes of RNA preserved tumors remained from dogs 2 and 3 after western blot analyses were performed, and use of FFPE canine brain tumor samples has been described previously for use with the with nCounter® instrument (NanoString Technologies, Inc., Seattle, WA, USA) and Canine Immuno-Oncology panel kit (Nanostring).[27] Representative H&E stained tissue sections were used to select ablated regions in post-treatment samples for mRNA analyses. For RNA isolation from FFPE, two 20 μm-thick scrolls from each sample were deparaffinized by incubation in xylene, followed submersion in 100% EtOH (10 min), 95% EtOH (10 min), 80% EtOH (10 min), and 75% EtOH (10 min), followed by a rinse in demineralized water. RNA from deparaffinized FFPE-tissue sections was extracted using the High Pure FFPET RNA Isolation Kit (Roche) according to the manufacturer's protocols. RNA concentration and quality were determined using the Nanodrop system. The extracted RNA was analyzed with nCounter® instrument and nSolver software (NanoString) and Canine Immuno-Oncology panel kit (Nanostring) to quantify expression of 800 genes across 47 annotated pathways following the manufacturer's protocol.[27]

Raw data from the nCounter® Canine Immuno-Oncology panel was uploaded to the ROSALIND® (ROSALIND, San Diego, CA, USA) cloud based software for normalization, and calculation of fold changes and p-values as recommended by Nanostring and described previously.[28] Housekeeping genes were selected for normalization based on the geNorm algorithm as implemented in the NormqPCR R library, and fold changes and p-values are calculated using the fast method. The Benjamini–Hochberg method of estimating false discovery rates (FDR) was used for p-value adjustment.[28] Ingenuity Pathway Analysis (IPA; Qiagen, Germantown, MD, USA) software was utilized for pathway analysis. IPA gene expression data were ranked based on z-score.

Results

Baseline Canine Subject and Tumor Characteristics

Three dogs with intracranial meningiomas were treated in the study (Table 1). All dogs presented with seizures attributable to their tumor, and the median duration of clinical signs prior to enrollment in the trial was 51 days (range, 41 to 74 days). Dog 1 also had focal interictal neurological deficits referable to the neuroanatomic location of the tumor in the brain. All dogs were receiving anticonvulsant medications (phenobarbital, levetiracetam, or both) and prednisone (median dose 0.78 mg/kg/day per os) at the time of enrollment, but had not received any other therapies.

Histotripsy Treatment

Histotripsy treatments were successfully applied to tumors of each dog (Table 2). Histotripsy treatment volumes were planned to be contained entirely within the tumor as confirmed via pre-treatment MRI to minimize the potential for off-target damage to surrounding healthy brain structures. A hyperechoic histotripsy cavitation bubble cloud in the treatment region on real-time ultrasound imaging was observed in dog 1 (Figures 3A and 3B), and intermittently in dog 3, although PCD confirmed the presence of histotripsy cavitation in the targeted region in all dogs.[9] Cavitation was maintained for the duration of the volumetric ablation in all treatments. In all three dogs, reflective distortions to the ultrasound image were caused by the sterile plastic coupling medium surrounding the therapy/imaging transducer assembly (Figure 3B). No significant changes in the echogenicity of the treated regions were observed when imaged with on coaxial ultrasound probe contained within histotripsy transducer assembly. Hypoechoic

Table 1. Canine Subject and Tumor Characteristics

Dog	Breed	Age (years)	Body Weight (kg)	Sex	Day −1 KPS	Tumor Location/Craniotomy Approach	Tumor Grade/Subtype
1	Field Spaniel	6	23	Male Neutered	80	Right temporal convexity/ Right rostrotentorial	I Angiomatous
2	Greyhound	11	25	Female Spayed	90	Right temporal convexity/ Right rostrotentorial	I Fibrous
3	Cockapoo	11	10	Female Spayed	90	Left frontotemporal convexity/ Left transzygomatic	I Microcystic

Table 2. Histotripsy Treatment Parameters and Outputs

Dog	Planned Treatment Volume (mm^3)	Free Field Treatment Pressure (mPa)	Treatment Duration (min)	Bubble Cloud Visualized	Passive Cavitation Detection Confirmed	Pre-focal Cavitation Observed
1	268.1; 8 mm diameter sphere	36.75	12.45	Yes	Yes	No
2	33.5; 4 mm diameter sphere	41.44	0.53	No	Yes	No
3	33.5; 4 mm diameter sphere	36.75	0.62	Intermittent	Yes	No

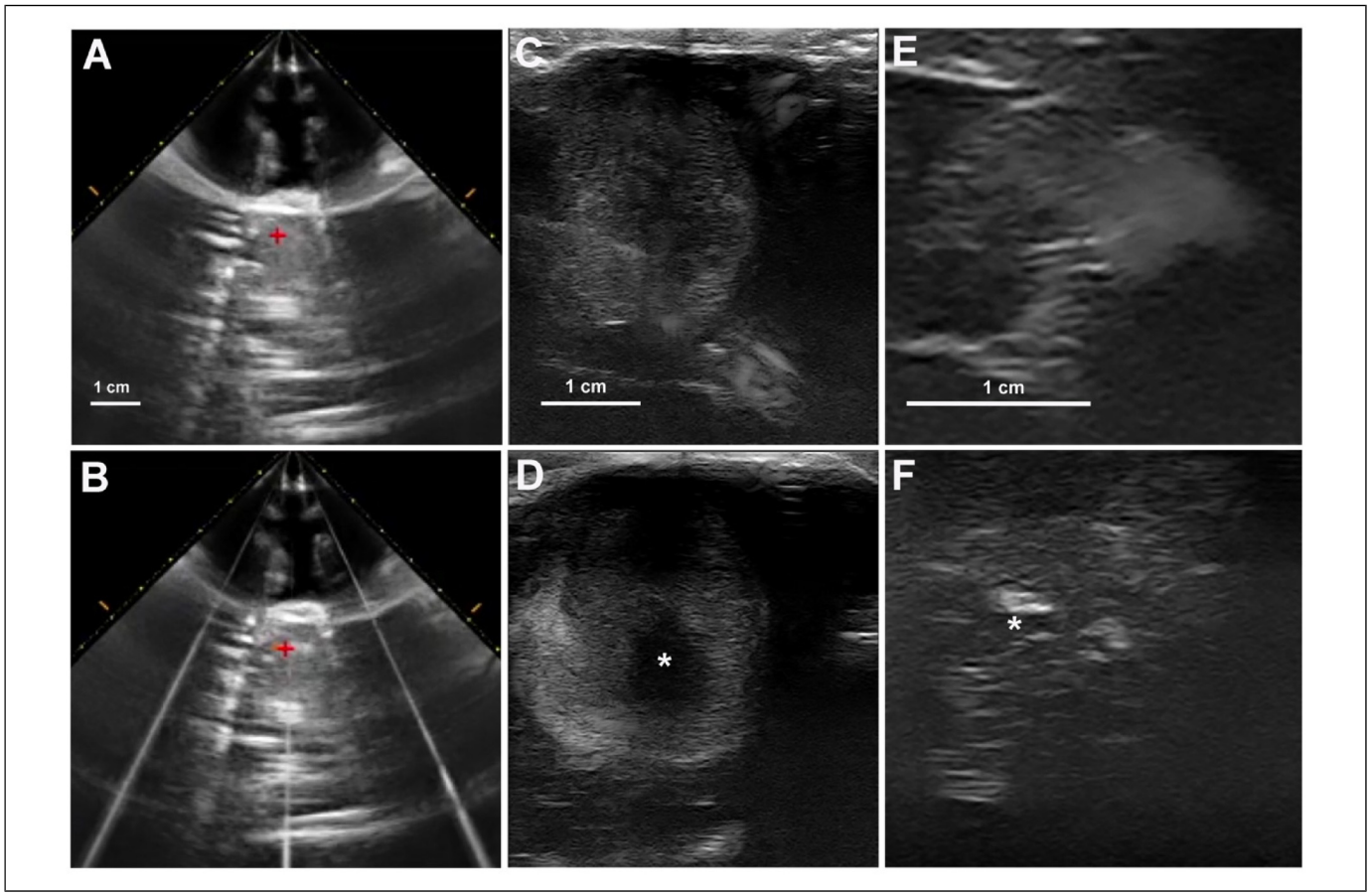


Figure 3. Real-time B-mode ultrasound imaging during histotripsy treatment. Pre-treatment tumor imaging using the coaxially aligned imaging probe within the transducer assembly (A; dog 1) and free-hand imaging using high-frequency linear probe (C; dog 1 and E; dog 2) in dog 1. A hyperechoic histotripsy bubble cloud (B; dog 1) can be seen during treatment in the targeted region (red +), but was difficult to visualize during due to reflections from the coupling medium. Ovoid hypoechoic zones (asterisks in D; dog 1 and F; dog 2) were observed following histotripsy treatment in using a freehand high frequency linear ultrasound probe. Pre-treatment images depicted in top row (A,C,E), and post-treatment images in bottom row (B,D,F).

(Figures 3C and 3D; dog 1) to mixed hypoechoic and hyperechoic regions (Figures 3E and 3F; dog 2) of ablation could be visualized in the treated region when using freehand ultrasound imaging using the high frequency linear probe. A distinct ablative lesion was not able to be visualized with ultrasound in dog 3.

MRI Treatment Assessments

Post-treatment MRI (day 0) were obtained a median of 48 min (range, 36 to 79 min) after completion of histotripsy treatment. In dogs 1 and 2, histotripsy ablations appeared as focal round to ovoid intratumoral lesions that were hypo- to mixed hypo- and hyperintense on T1 W (Figure 4A), uniformly hypointense or mixed hypointense on T2 W and FLAIR (Figures 4A and 4B), and hypointense (non-enhancing) to isointense on post-contrast T1 W (Figure 4B) sequences.

In dog 3, a discrete histotripsy lesion could not be definitively identified on post-treatment MRI. Histotripsy lesions quantified by MRI were smaller than planned volumes (Table 3). On post-treatment MRI, there was no evidence of off-target lesions in the brains of dogs 1 and 2, but exacerbation of pre-existing peritumoral cerebral edema (neurologic AE, Grade 3) that was possibly attributable to the histotripsy was observed in dog 3 (Figure 4C; Supplemental Figure S2). The median time from application of histotripsy treatment to completion of tumor resection was 2.7 h (range 2.3-4.5 h). On day 42 MRI, dogs 1 and 3 had evidence of gross total tumor resection (no tumor present), and dog 2 had evidence of progressive disease characterized by an 86% increase in the CEV compared to the day −1 MRI (Table 3; Figure 4). The cerebral edema present in dog 3 was resolved on the day 42 MRI.

Clinical Safety Primary Endpoint

All dogs completed the 42 day study period. The peritumoral cerebral edema in dog 3 was associated with a 10 point decline in the KPS score due to right sided muscle weakness (neurologic AE, Grade 2) that was apparent on day 1 and remained static until discharge on day 3. On the day 14 recheck the right sided weakness was present but improved. Dogs 1 and 2 did not experience any adverse events, and the KPS score of dog 2 remained static over the course of the study. The KPS of dog 1 improved to 90 at the 14 day recheck and remained static at 42 days.

Feasibility Primary Endpoint- Tumor Pathology and Morphometry

Histotripsy ablations manifested grossly as round hemorrhagic and malacic foci in sectioned tumors of dogs 1 and 2 (Figure 5A). Microscopically, ablations appeared as circular (dogs 1 and 2) or irregularly shaped (dog 3) areas of amorphous cellular debris with few intact neutrophils and lymphocytes scattered throughout the debris field and multiple foci of intact erythrocytes within the interstitium (Figures 5B and 5C). Lesions were sharply demarcated from surrounding untreated tumor tissue. Intensely acidophilic and shrunken tumor and stromal cellular cells and vascular ghosts were frequently observed at the border of treated and untreated regions (Figure 5D). Measured ablations were slightly smaller than planned sizes, with HAV of 242 mm^3, 29 mm^3, and ~17 mm^3 dogs 1 and 2, and 3, respectively. In dog 3, the ablated region extended into a

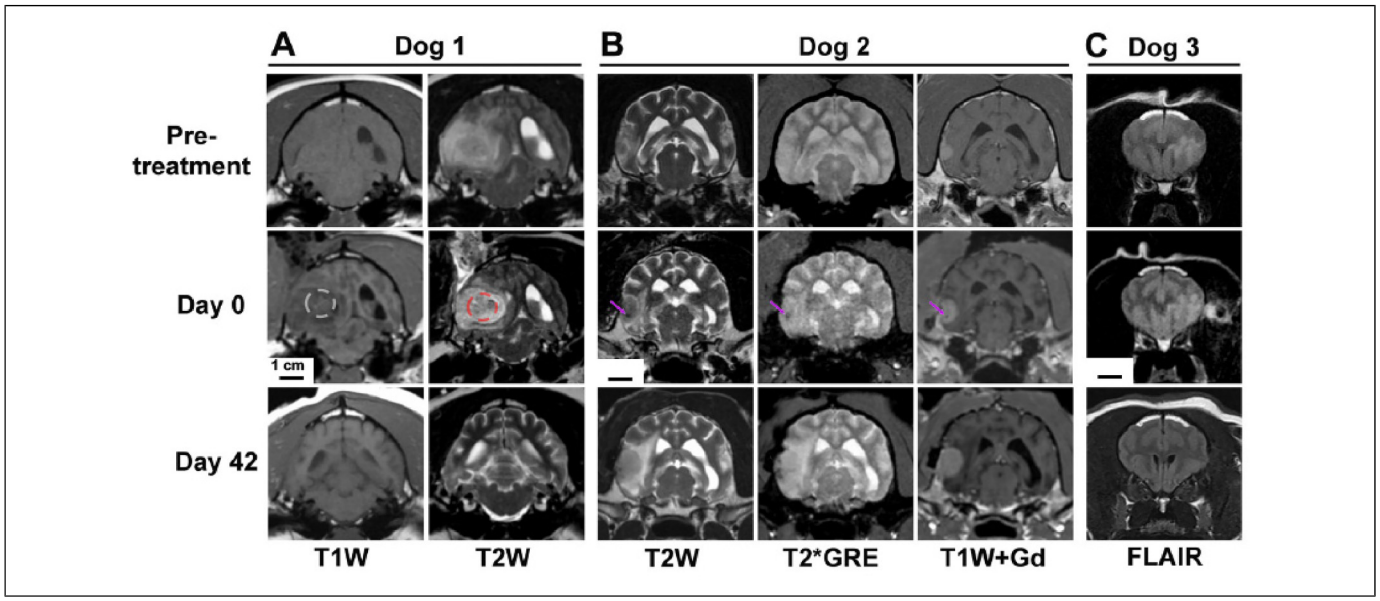


Figure 4. MRI characteristics of histotripsy ablations. Histotripsy ablations appear as focal round to ovoid lesions that are T1 W hyperintense (A; white broken circle), mixed T2 W hypointensity (A; red broken circle) or uniformly hypointense lesions on T2 W, T2*GRE and post-contrast images (B; purple arrows). In dog 2, tumor progression was noted on day 42 (B). Treatment associated exacerbation of cerebral edema was observed in dog 3 (C) which resolved by day 42. Bar = 1 cm in all panels.

Table 3. MRI Derived Outcomes for Histotripsy Treated Tumors

Dog	Pre-treatment CEV (mm^3)	Planned Treatment Volume (mm^3)	Day −1 CEV (mm^3)	mHLV (mm^3)	Max 2D Lesion Diameter (mm)	Day 42 CEV (mm^3)
1	5079	268.1; 8 mm diameter sphere	5117	205	6.4	0
2	291	33.5; 4 mm diameter sphere	497	19	3.2	923
3	586	33.5; 4 mm diameter sphere	574	ND	ND	0

CEV = contrast-enhancing tumor volume.
mHLV = MRI-derived histotripsy lesion volume.
ND = not determined.

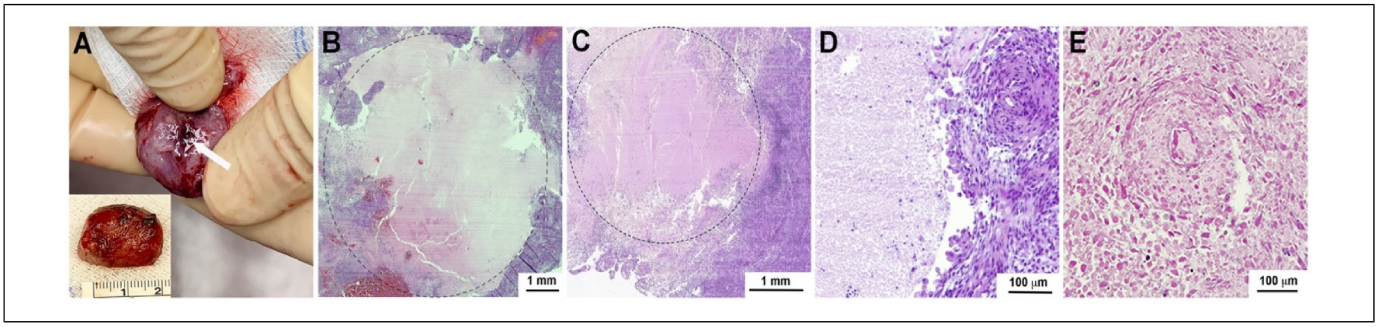


Figure 5. Pathologic features of histotripsy ablations. Treated regions appeared as hemorrhagic and malacic foci (A; arrow, dog 1) on cut surface of tumors following resection. Microscopically (B-E), ablations consisted of circular pale and largely acellular debris fields with scattered foci of hemorrhage that were clearly demarcated from untreated tumor. Broken circles in B (dog 1) and C (dog 2) represent planned 8 mm and 4 mm diameter ablations, corresponding to histologic ablation volumes of 242 mm^3 and 29 mm^3, respectively. In some areas at the border between treated and untreated tumor, intensely eosinophilic tumor, vascular, and stromal cells were noted (D and E, dog 3). Centimeter scale bar depicted in A inset. Hematoxylin and eosin stain in panels B-E.

cystic cavity and to the surface of the tumor capsule which were artifactually disrupted during sectioning which precluded accurate quantification of the HAV.

Exploratory Immunologic Assessments

- ***Plasma and Intratumoral HMGB1***

Plasma HMGB1 concentrations in healthy dogs did not change over time, and were significantly lower compared to dogs with meningiomas ($p < 0.01$; Figure 6A). Plasma HMGB1 concentrations were not significantly different between dogs with meningiomas treated surgically and those treated with histotripsy and surgery. In dogs with meningiomas, day 1 post-treatment plasma HMGB1 concentrations were increased compared to pre-treatment values, but differences were not statistically significant. Day 14 and 42 post-treatment plasma HMGB1 concentrations were significantly lower ($p < 0.02$) compared to pre-treatment and day 1 post-treatment HMGB1 concentrations in dogs with meningiomas treated with surgery and with histotripsy and surgery. Intratumoral expression of HMGB1 increased significantly ($p = 0.03$) in tumor samples following histotripsy treatment (Figures 6B and 6C).

- ***Tumor Immunohistochemistry***

Significant differences in numbers of immunolabeled cells were not detected between pre- and post-treatment tumor samples for any of the antibodies evaluated (Figure 7A). In pre-treatment tumor samples, immunolableled CD3, CD4, CD8, CD79a, FoxP3, and MHCII cells were identified scattered throughout the tumor bulk (Figure 7B), and Iba-1 immunolabeled cells were mainly found at tumor-brain and tumor capsular interfaces. Cells that demonstrated iNOS immunolabeling were rarely observed in the tumor mass of pre-treatment biopsies of dogs 1 and 3, and were not detected in post-treatment tumors samples from any dog. In post-treatment tumor samples, CD3, CD4, CD8, CD79a, and FoxP3 immunolabeled cells were predominantly found at the transition between treated and untreated tumor. Ablated regions were largely devoid of immunolabeled cells, with the exception of perivascular cuffs of $CD3^+/CD8^+$ cells (Figure 7C and 7D) and lesser numbers of perivascular $MHCII^+$ cells (Figure 7E).

- ***Tumor Gene Expression***

Comparative analyses of pre- and post-treatment tumors revealed 99 significantly differentially expressed genes, including 94 upregulated and 5 downregulated genes (Figure 8A; Supplemental Tables S2 and S3). Genes that were enriched included those involved in intrinsic signaling pathways associated with tumorigenesis and cancer progression, cellular metabolism stress, and death, and those involved in immune responses (Figures 8B and 8C). In post-treatment tumors, there were trends for enrichment of neutrophil, dendritic cell, macrophage, and cytotoxic T cell immune signatures, but these were not statistically significant (Figure 8D).

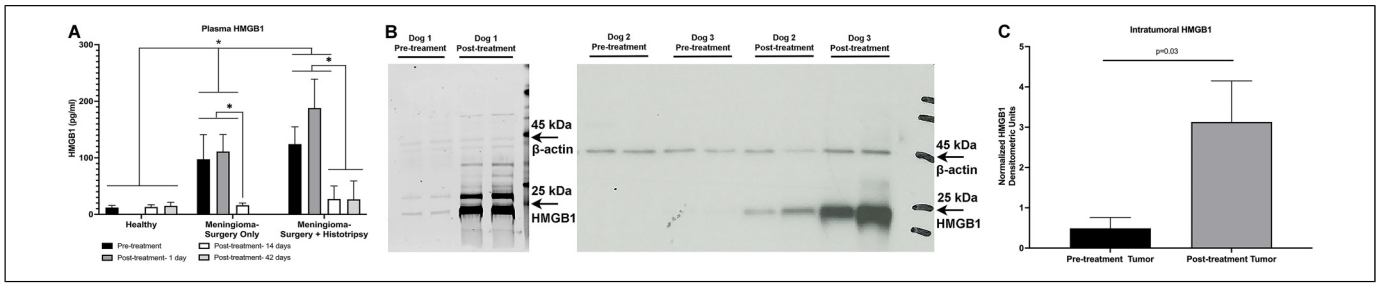


Figure 6. Plasma and intratumoral HMGB1 concentrations. Plasma HMGB1 concentrations (A) are significantly elevated in dogs with meningiomas compared to healthy dogs. Plasma HMGB1 concentrations transiently increase in dogs with meningiomas following histotripsy treatment, but post-treatment increases in plasma HMGB1 were not significantly different compared to dogs treated with conventional surgery only. Compared to pre-treatment (untreated) tumor samples, intratumoral expression of HMGB1 increased significantly (B, C) in all dogs following histotripsy treatment, as determined via western blotting.

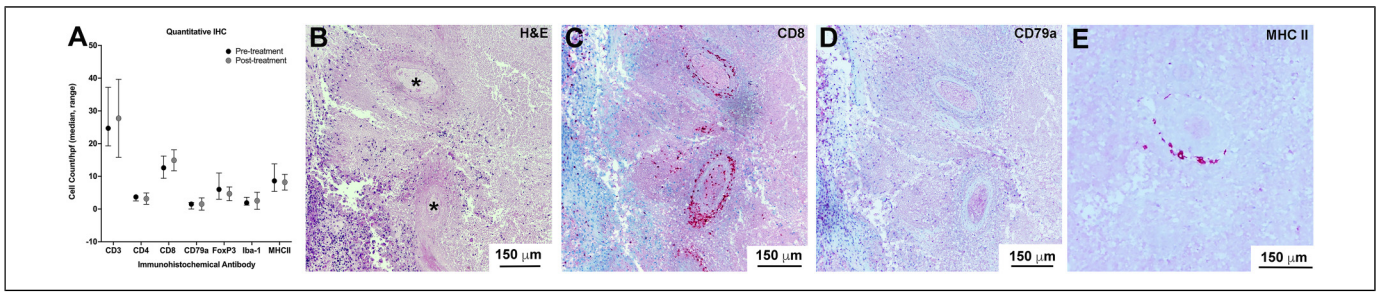


Figure 7. Meningioma immunohistochemistry. Quantitative differences in tumor immune cell populations (A) were not observed between pre- and post-treatment samples. Hematoxylin and eosin (H&E) stained section (B; dog 2) illustrating transition area between untreated, viable tumor (left side of panel) and histotripsy ablated tumor (right side of panel), with vascular profiles (*) delineated within the ablated regions. Intra-and peri-vascular cuffs (C; dog 2) of CD8 immunolabeled lymphocytes can be seen in the ablated region of tumor. Near total absence of CD79a immunolableled lymphocytes in ablated region of tumor (D; dog 2), with representative positive CD79a immunolabeled cells apparent in the transition area to the left of the panel. Perivascular cuffs of MHCII immunolabeled cells (E; dog 3) were also present in post-treatment tumor samples.

Discussion

This study demonstrates the feasibility and safety of ultrasound-guided histotripsy treatment of spontaneous brain tumors using an open craniectomy approach. Histotripsy treatments were successfully delivered and monitored using intraoperative ultrasound (ioUS) imaging and PCD, and ablative lesions could be visualized on post-treatment MRI and neuropathologic examinations. The histotripsy treatments were not associated with any unexpected or serious adverse events. Although histotripsy has been used for the ablation of multiple tumor types, its utility for treating brain tumors remains to be defined.[7–9] Studies investigating the feasibility of transcranial histotripsy are currently limited by the need for advanced histotripsy devices able to overcome attenuation of ultrasound by the skull and capable of incorporating MRI guidance, leaving an immediate unmet clinical need and opportunity to develop other histotripsy approaches to brain tumor treatment.[10,11]

The current trial attempts to bridge this gap and advance the translation of histotripsy by establishing an alternative, accessible, and minimally invasive solution using readily available histotripsy devices and ioUS guidance, which is widely used in contemporary neurosurgical practice.[29] Target tumors were clearly visible on freehand and coaxial ultrasound in the dogs following craniectomy, guiding the proper alignment of the histotripsy transducer without need for additional MRI or image fusion. During treatment, histotripsy bubble clouds were generated within the targeted regions in all dogs, but the bubble cloud could only be seen consistently with coaxial ioUS in one dog, resulting in the use of PCD to monitor cavitation activity at or near the focus in the other two dogs. While real-time bubble cloud monitoring using ioUS is desirable for all histotripsy treatments, ioUS visualization of bubble clouds in two dogs in this study represents an improvement over MRI-guided histotripsy studies for brain ablation, where no real-time feedback was available.[10] Notably, significant changes in the echogenicity of the treated tumor were unable to be discerned immediately post-treatment in any of the dogs using the coaxial ioUS imaging probe, but a hypoechoic ablation zone was visible when using freehand imaging with a high frequency linear probe. It is expected that refinements in the histotripsy treatment system that incorporate higher resolution ioUS imaging transducers and optimized acoustic coupling methods that minimize imaging artifact will overcome these limitations and allow for visualization of bubble clouds and

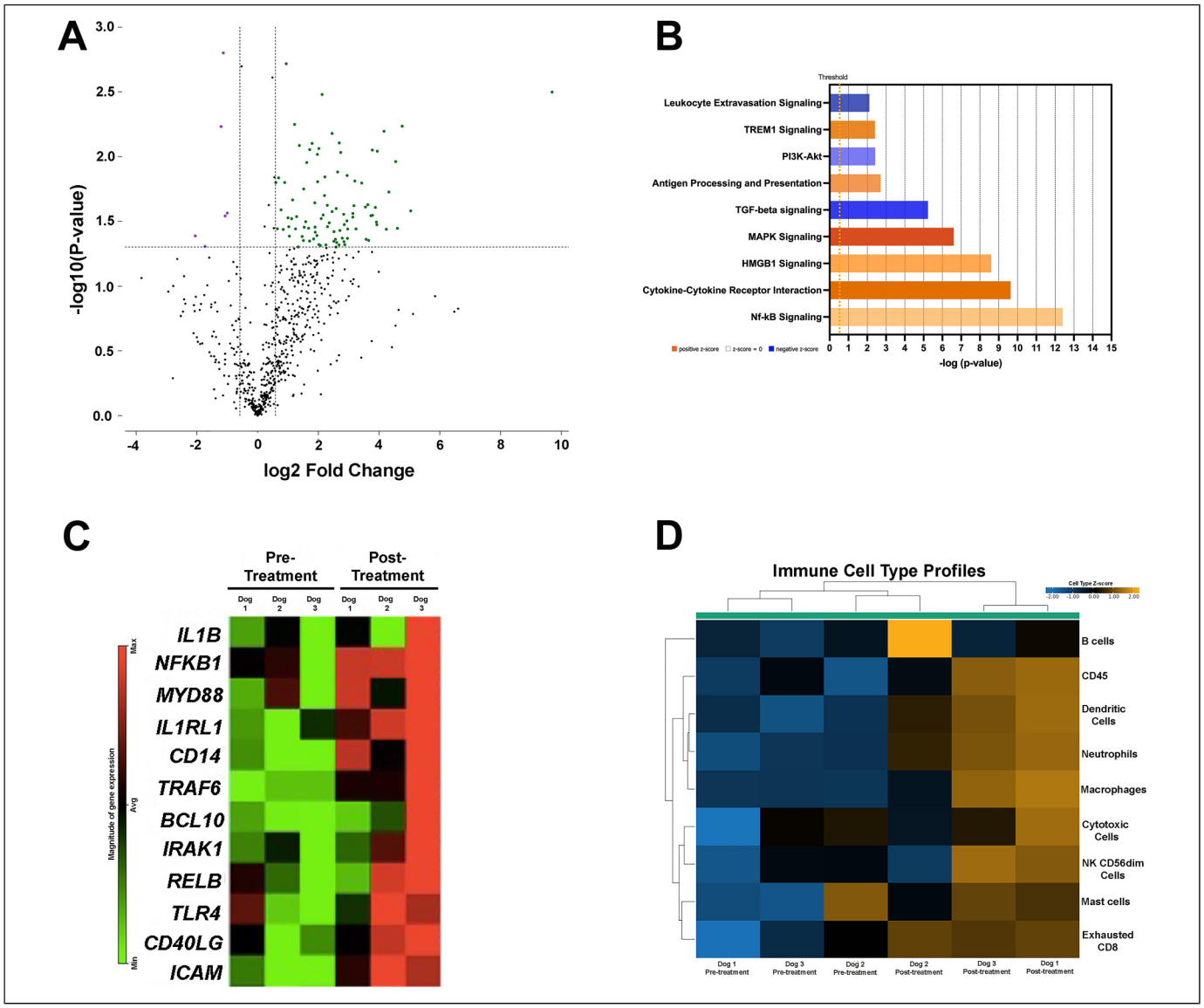


Figure 8. Gene expression of meningiomas treated with histotripsy. Volcano plot (A) of differentially expressed genes between tumors pre- and post-treatment. Ninety-four genes were significantly upregulated (green) and five (purple) were significantly downregulated following treatment. The canonical pathways (B) most significantly impacted by histotripsy treatment. NF-κB signaling was the top pathway influenced by histotripsy (B), with comparative expression of genes involved in this pathway across dogs and treatment conditions depicted in the heatmap (C). Significant differences in immune cell profiles (D) were not observed between tumors before or after histotripsy. For panels A, B, and D p-value thresholds were set at 0.05.

treatment induced tissue changes in the majority of patients.[29,30] These challenges have also been previously recognized when evaluating histotripsy for neurosurgical applications, resulting in development and validation of high frequency, minimally invasive histotripsy systems.[30]

Histotripsy lesions were identifiable on post-treatment MRI scans in dogs 1 and 2, appearing as well demarcated lesions that corresponded with targeted locations and approximated planned treatment volumes. The characteristics of histotripsy lesions on multiparametric MRI sequences observed in this study were consistent with published MRI descriptions of histotripsy treatment in normal animal brains.[10,31] Histotripsy treated regions of canine meningiomas appeared hypo- to hyperintense on T1 W, hyper- to hypointense on T2 W, hypointense of T2*GRE, and iso to hypointense on post-contrast T1 W sequences, which are features compatible with corresponding histopathological evidence of necrosis and intralesional hemorrhage in this and previous studies.[10,31] The more mixed MRI appearances of lesions seen in the dogs is likely attributable to intrinsic heterogeneity of tumors compared to normal cerebrum, as well as the fact that meningiomas arise outside of the blood-brain barrier and thus typically demonstrate marked contrast enhancement.[4,15] The inability to visualize a distinct ablation zone on MRI or ioUS in dog 3 was attributed to collapse of a cystic cavity during treatment.

Pathological examination of treated tumors confirmed the feasibility of the histotripsy treatment and findings noted on post-treatment ultrasound and MRI. Histotripsy ablations could be visualized macroscopically in treated tumors, appearing as foci of malacia and hemorrhage. Histopathological examinations revealed complete disruption of targeted tumor regions, with ablated areas consisting of necrotic cellular and amorphous debris and regions of intra- and perilesional hemorrhage, findings similar to those previously reported in histotripsy treated normal brain.[10,31] Quantitative HAV corresponded closely with planned treatment volumes in the 2 dogs in which they could be assessed, and clearly defined boundaries between untreated and treated tumor regions were observed in all cases. The effective histotripsy dose of 400 pulses per treatment location utilized in this study was chosen based on previous histotripsy studies for other soft tissue applications, and the considerably higher mechanical strength of human meningiomas compared to healthy brain tissue.[7–10,32] Based on the histological lesions observed in the targeted tumors, and the success of lower histotripsy doses in achieving $\geq 90\%$ destruction of healthy brain tissue (50-200 pulses per point), it is possible that 400 pulses per point resulted in overtreatment of canine meningiomas.[10,31] Future studies should consider the optimized treatment dose for this application, particularly for large tumor volumes.

In this study, histotripsy was generally well tolerated, although dog 3 developed an AE characterized by transient neurological deterioration secondary to an exacerbation of cerebral edema that was possibly attributable to histotripsy treatment. Mild perilesional edema has been reported following histotripsy ablation of normal porcine brain, so this AE was not completely unexpected.[31] It is possible that presence of a macroscopic intratumoral cyst or pre-existing edematous brain in this dog made it more susceptible to the mechanical effects of histotripsy. The potential risk associated with developing cerebral edema could have important implications in the future translation of the technology if the intended indications include complete tumor ablations, or treatment of margins at the brain-tumor interface. The experience in dog 3 also suggests that caution is advised when selecting patients with cystic tumors for histotripsy treatment.

Exploratory immunological analyses were performed in this study in consideration of the emerging evidence that histotripsy can cause immunogenic cell death and abscopal tumor responses in systemic cancers, coupled with the serious clinical need for improved immunotherapeutics for central nervous system tumors.[33–35] In the canine meningiomas analyzed here, encouraging preliminary evidence of histotripsy associated immune responses were observed, including increased intratumoral expression of HMGB1, and upregulation of diverse but functionally related immune pathways such as DAMP signaling, antigen presentation, cytokine-cytokine receptor interaction, and NF-κb signaling pathways. Similar patterns in gene expression and pathway activation have been observed in other studies of histotripsy treated murine tumors.[33,35] In this study, peripheral blood HMGB1 concentrations were higher in dogs with meningiomas than healthy dogs, but significant difference in plasma HMGB1 concentrations in dogs with meningiomas treated with histotripsy compared to those treated with conventional surgery alone were not detected. It is known that trauma will increase plasma HMGB1 concentrations in dogs, so these data are not surprising in the face of surgical trauma.[36] Given the short plasma half-life ($\sim$17 min) of HMGB1, it is possible that the 1 day post-treatment sampling point used in this study did not capture peak plasma HMGB1 concentrations.[37] Significant differences in the numbers or types of infiltrating immune cells nor inferred immune cell gene expression profiles were not observed between pre- and post-treatment tumors, but the acute nature of the treat and resect study design used here likely mitigated our ability to detect genomic and adaptive immune responses in the tumor microenvironment associated with histotripsy treatment. Further characterization of histotripsy ablation and immune responses will likely require allowing tumors to remain *in situ* for longer periods following treatment before analyses.

Additional limitations of this study included the size and geometry of the histotripsy transducer assembly and acoustic coupling bath which presented challenges to adapting the technology to variably sized canine heads and targeting tumors located in areas of skull curvatures. The technical imaging and treatment capabilities of the histotripsy system used in this trial also precluded us from robustly investigating the utility of the ATCI in an attempt to apply the technology in ioUS guided transcranial applications.[19–21] However, these issues would likely be less relevant in translational context, given the convex shape and size of the human head.

Further, a small and homogenous convenience sample of tumors were partially treated in this study, such that the safety and feasibility of ablating other brain tumor histologies, including intraparenchymal tumors, or attempting to achieve complete tumor ablations remain unknown. To overcome these limitations and further advance histotripsy for brain tumors, we and others have designed integrated histotripsy transducers with smaller footprints, higher frequency imaging probes and more powerful therapeutic transducer elements, that can be coupled to the patient using disposable, commercial ultrasound transducer covers to be used in future intracranial histotripsy treatments.[30]

Conclusions

In a large animal spontaneous brain tumor model, ultrasound-guided histotripsy tumor ablation through an open craniectomy window was demonstrated to be feasible and safe. Histotripsy induced lesions could be visualized on post-treatment ultrasonographic, MRI, and pathological studies, with treated regions representative of planned volumes. This study provides novel data regarding the clinical and neuropathological effects of histotripsy in the naturally diseased brain, which are important for future investigational study designs and translation of the technology for neurological indications.

Abbreviations

AE	adverse events
CEV	contrast-enhancing tumor volume
DAMP	damage associated molecular patterns
FOPH	fiber optic probe hydrophone
HMGB1	high mobility group box 1
ioUS	intraoperative ultrasound
HAV	histologic ablation volume
KPS	Karnofsky Performance Score
mHLV	MRI derived histotripsy lesion volume
MRI	magnetic resonance imaging
PCD	passive cavitation detection
PRF	pulse repetition frequency

Acknowledgements

Author Lauren Ruger was supported by the Virginia Tech Institute for Critical Technology and Applied Science (ICTAS) Doctoral Scholars program throughout the duration of this work. Author Rell Parker is an iTHRIV Scholar. The iTHRIV Scholars Program is supported in part by the National Center for Advancing Translational Sciences of the National Institutes of Health under Award Numbers UL1TR003015 and KL2TR003016.

Data Availability

Gene expression data can be accessed on the Mendeley data repository: Rossmeisl, Jr., John (2024), "FIDOHIST Trial Data", Mendeley Data, V1, doi: 10.17632/dk73vxpdmc.1
Proteomic and immunohistochemical data is available in supplemental file: "Supplementary File- Proteomic and Immunohistochemical Data.xlsx".

Declaration of Conflicting Interests

The author(s) declared the following potential conflicts of interest with respect to the research, authorship, and/or publication of this article: Lauren Ruger has an ongoing consulting relationship with Theraclion, and Eli Vlaisavljevich has an ongoing research partnership and financial relationship with HistoSonics, Inc. Jonathan Sukovich, Timothy Hall, and Zhen Xu have financial conflicts with Histosonics, Inc.

Funding

The author(s) disclosed receipt of the following financial support for the research, authorship, and/or publication of this article: This work was funded by the Focused Ultrasound Foundation, grant #FUS848, and the American Kennel Club Canine Health Foundation, grant #2907.

Ethics Statement

The canine study was approved by the Virginia Tech Institutional Animal Care and Use Committee, protocol 20-190, approved November 20, 2020.

ORCID iDs

Elliana Vickers https://orcid.org/0000-0003-2639-9470
John H. Rossmeisl https://orcid.org/0000-0003-1655-7076

Supplemental Material

Supplemental material for this article is available online.

References

1. Ostrom QT, Price M, Neff C, et al. CBTRUS Statistical report: Primary brain and other central nervous system tumors diagnosed in the United States in 2016–2020. *Neuro Oncol*. 2023;25(12 Suppl 2):iv1–iv99.
2. Dincer A, Morales-Valero SF, Robert SM, et al. Surgical strategies for intracranial meningioma in the molecular era. *J Neurooncol*. 2023;162(2):253–265.
3. Karschnia P, Young JS, Dono A, et al. Prognostic validation of a new classification system for extent of resection in glioblastoma: A report of the RANO *resect* group. *Neuro Oncol*. 2023;25(5):940–954.
4. Miller AD, Miller CR, Rossmeisl JH. Canine primary intracranial cancer: A clinicopathologic and comparative review of glioma, meningioma, and choroid plexus tumors. *Front Oncol*. 2019; 9:1151.
5. LeBlanc AK, Mazcko C, Brown DE, et al. Creation of an NCI comparative brain tumor consortium: Informing the translation of new knowledge from canine to human brain tumor patients. *Neuro Oncol*. 2016;18(9):1209–1218.
6. Xu Z, Hall TL, Vlaisavljevich E, Lee Jr FT. Histotripsy: The first noninvasive, non-ionizing, non-thermal ablation technique based on ultrasound. *Int J Hyperthermia*. 2021;38(1):561–575.
7. Vidal-Jove J, Serres X, Vlaisavljevich E, et al. First-in-man histotripsy of hepatic tumors: The THERESA trial, a feasibility study. *Int J Hyperthermia*. 2022;39(1):1115–1123.
8. Schade GR, Keller J, Ives K, et al. Histotripsy focal ablation of implanted prostate tumor in an ACE-1 canine cancer model. *J Urol*. 2012;188(5):1957–1964.
9. Ruger LN, Hay AN, Vickers ER, et al. Characterizing the ablative effects of histotripsy for osteosarcoma: In vivo study in dogs. *Cancers (Basel)*. 2023;15(3):741.
10. Lu N, Gupta D, Daou BJ, et al. Transcranial magnetic resonance-guided histotripsy for brain surgery: Pre-clinical investigation. *Ultrasound Med Biol*. 2022;48(1):98–110.
11. Sukovich JR, Macoskey JJ, Lundt JE, et al. Real-time transcranial histotripsy treatment localization and mapping using acoustic cavitation emission feedback. *IEEE Trans Ultrason Ferroelectr Freq Control*. 2020;67(6):1178–1191.
12. Percie du Sert N, Hurst V, Ahluwalia A, et al. The ARRIVE guidelines 2.0: Updated guidelines for reporting animal research. *Br J Pharmacol*. 2020;177(16):3617–3624.
13. Valladao ML, Scarpelli KC, Metze K. Clinical utility of a life quality score in dogs with canine transmissible venereal tumor treated by vincristine chemotherapy. *Arq Bra Med Vet Zootec*. 2010;62(5):1086–1093.
14. Latouche EL, Arena CB, Ivey JW, et al. High-frequency irreversible electroporation for intracranial meningioma: A feasibility study in a spontaneous canine tumor model. *Technol Cancer Res Treat*. 2018;17:1533033818785285.
15. May JL, Garcia-Mora J, Edwards M, et al. An illustrated scoping review of the magnetic resonance imaging characteristics of canine and feline brain tumors. *Animals (Basel)*. 2024;14(7):1044.

16. LeBlanc AK, Atherton M, Bentley RT, et al. Veterinary cooperative oncology group-common terminology criteria for adverse events (VCOG-CTCAE v2) following investigational therapy in dogs and cats. *Vet Comp Oncol*. 2021;19(2):311–352.
17. Rossmeisl JH, Herpai D, Quigley M, et al. Phase I trial of convection-enhanced delivery of IL13RA2 and EPHA2 receptor targeted cytotoxins in dogs with spontaneous intracranial gliomas. *Neuro Oncol*. 2021;23(3):422–434.
18. Packer RA, Rossmeisl JH, Kent MS, et al. Consensus recommendations on standardized magnetic resonance imaging protocols for multicenter canine brain tumor clinical trials. *Vet Radiol Ultrasound*. 2018;59(3):261–271.
19. Ruger L, Langman M, Farrell R, et al. Ultrasound-guided mechanical high-intensity focused ultrasound (Histotripsy) through an acoustically permeable polyolefin-based cranioplasty device. *IEEE Trans Biomed Eng*. 2024. doi: 10.1109/TBME.2024.3399688, epub ahead of print.
20. Librizzi L, Uva L, Raspagliesi L, et al. Ultrasounds induce blood-brain barrier opening across a sonolucent polyolefin plate in an in vitro isolated brain preparation. *Sci Rep*. 2022;12(1):2906.
21. Prada F, Franzini A, Moosa S, et al. In vitro and in vivo characterization of a cranial window prosthesis for diagnostic and therapeutic cerebral ultrasound. *J Neurosurg*. 2020;134(2):646–658.
22. Garcia Mora JK, Robertson J, Hsu FC, et al. Comparison of linear and volumetric criteria for the determination of therapeutic response in dogs with intracranial gliomas. *J Vet Intern Med*. 2022;36(3):1066–1074.
23. Belluco S, Marano G, Baiker K, et al. Standardisation of canine meningioma grading: Inter-observer agreement and recommendations for reproducible histopathologic criteria. *Vet Comp Oncol*. 2022;20(2):509–520.
24. Imran KM, Ganguly A, Paul T, et al. Magic bubbles: Utilizing histotripsy to modulate the tumor microenvironment and improve systemic anti-tumor immune responses. *Int J Hyperthermia*. 2023; 40(1):2244206.
25. Partridge BR, O'Brien TJ, Lorenzo MF, et al. High-frequency irreversible electroporation for treatment of primary liver cancer: A proof-of-principle study in canine hepatocellular carcinoma. *J Vasc Interv Radiol*. 2020;31(3):482–491.e4.
26. Boozer LB, Davis TW, Borst LB, et al. Characterization of immune cell infiltration into canine intracranial meningiomas. *Vet Pathol*. 2012;49(5):784–795.
27. Chambers MR, Foote JB, Bentley RT, et al. Evaluation of immunologic parameters in canine glioma patients treated with an oncolytic herpes virus. *J Transl Genet Genom*. 2021;5(4):423–442.
28. Magee K, Marsh IR, Turek MM, et al. Safety and feasibility of an in situ vaccination and immunomodulatory targeted radionuclide combination immuno-radiotherapy approach in a comparative (companion dog) setting. *PLoS One*. 2021;16(8):e0255798.
29. Prada F, Ciocca R, Corradino N, et al. Multiparametric intraoperative ultrasound in oncological neurosurgery: A pictorial essay. *Front Neurosci*. 2022;16:881661.
30. Landry TG, Gannon J, Vlaisavljevich E, et al. Endoscopic coregistered ultrasound imaging and precision histotripsy: Initial *in vivo* evaluation. *BME Front*. 2022;2022:9794321.
31. Sukovich JR, Cain CA, Pandey AS, et al. In vivo histotripsy brain treatment. *J Neurosurg*. 2018;131(4):1331–1338.
32. Stewart DC, Rubiano A, Dyson K, et al. Mechanical characterization of human brain tumors from patients and comparison to potential surgical phantoms. *PLoS One*. 2017;12(6):e0177561.
33. Pepple AL, Guy JL, McGinnis R, et al. Spatiotemporal local and abscopal cell death and immune responses to histotripsy focused ultrasound tumor ablation. *Front Immunol*. 2023; 14:1012799.
34. Vidal-Jové J, Serres-Créixams X, Ziemlewicz TJ, et al. Liver histotripsy mediated abscopal effect—case report. *IEEE Trans Ultrason Ferroelectr Freq Control*. 2021;68(9):3001–3005.
35. Eranki A, Srinivasan P, Ries M, et al. High-Intensity focused ultrasound (HIFU) triggers immune sensitization of refractory murine neuroblastoma to checkpoint inhibitor therapy. *Clin Cancer Res*. 2020;26(5):1152–1161.
36. Goggs R, Letendre JA. High mobility group box-1 and pro-inflammatory cytokines are increased in dogs after trauma but do not predict survival. *Front Vet Sci*. 2018; Jul 30, 5:179.
37. Zandarashvili L, Sahu D, Lee K, et al. Real-time kinetics of high-mobility group box 1 (HMGB1) oxidation in extracellular fluids studied by in situ protein NMR spectroscopy. *J Biol Chem*. 2013;288(17):11621–11627.